Molecular heterogeneity and differential metabolic signatures in thymic adipocytes

Joon Schwakopf,[1,2,3], Amber R. Syage,[1,3], Anca Franzini,[3,4], Katherine E. Varley,[3,4], Dean Tantin,[1,4]

[1]Department of Pathology, University of Utah School of Medicine, Salt Lake City, UT, USA.
[2]Department of Neurobiology, University of Utah School of Medicine, Salt Lake City, UT, USA.
[3]Huntsman Cancer Institute, University of Utah School of Medicine, Salt Lake City, UT, USA.
[4]Department of Oncological Sciences, University of Utah School of Medicine, Salt Lake City, UT, USA.

Correspondence: dean.tantin@path.utah.edu

Short title: Molecular characterization of thymic adipocytes

Keywords Thymus; T cells; Thymic epithelial cells; adipocytes; aging

Conflicts of interest statement: The authors have declared that no conflict of interest exists

Words in abstract: 180
Words main text: 5,610
Total main display items: 6

SUMMARY

Adipocyte depots throughout the body are physiologically and molecularly distinct. With age, adipocytes increase in and around aged thymi. However, thymic adipocytes completely lack molecular characterization. We developed and optimized methods to isolate adipocyte nuclei from mouse thymi of different ages and sexes. Single-nucleus multiomic analysis of male and female mice aged 4-9 months reveals that thymic adipocytes are heterogeneous, with at least two distinct populations. One subpopulation harbors a transcription and chromatin signature consistent with beige/brown fat. A larger subpopulation more strongly resembles classic white adipose tissue and expresses genes associated with epithelial-to-mesenchymal transition (EMT) and antigen presentation. Analysis of differentially open chromatin in the white compared to beige adipose population identifies binding sites for Foxn1 and HIF-1α/Arnt, consistent with a situation in which thymic white adipose cells emerge from thymic epithelial cells, possibly under hypoxic conditions. Immunofluorescence microscopy confirmed the expression of UCP1 protein in cells within the thymic parenchyma, most prominently in subcapsular cortical regions. This resource reveals a complex milieu of thymic adipocytes and identifies multiple avenues for directly probing their ontogeny, dynamics and functional significance.

KEYWORDS

Thymus; Adipocytes; Beige Fat; PPARα; UCP1

INTRODUCTION

The thymus is the primary site of T cell development and education and thus plays a central role in adaptive immunity and central tolerance [1]. It is a complex organ that consists of developing T cells (thymocytes), thymic epithelial cells (TECs), fibroblastic stromal cells, macrophages, dendritic cells (DCs), B cells (particularly in the medullar), mature nonconventional T cells (e.g., iNKTs), endothelial cells, pericytes, nerves, and other less abundant cell types. The aging thymus also accumulates abundant and dynamic population of adipocytes [1], which we here term ThyAds.

With age, areas of the thymus devoted to thymopoiesis atrophy and T cell output declines in a process termed thymic involution [2,3]. Involution is associated with progressive disruption of the cortico-medullary junction, loss of thymic output, and increased adiposity in a manner influenced by biological sex and diet [4]. Attenuation of thymic output contributes to reduced TCR diversity, impaired pathogen response and increased susceptibility to infection [1,5-9]. Additionally, involution can be accelerated by administration of thiazolidinediones, implicating adipocyte expansion in this process [10], however their function in this process is unclear. Thymic involution is conserved across vertebrates and recapitulated in laboratory mice. Although severe infection, radiation, malnutrition, or hormonal alterations can induce acute thymic atrophy, age-related involution is the setting in which adipocyte accumulation is most consistently observed [1,4,11-13]. Despite their increasing abundance in the aging thymus, and the possibility that they have specialized functions analogous to other tissue-specific fat depots [14], ThyAds have yet been directly studied at the molecular level. Prior studies focused on thymocytes and thymic stromal cells have omitted ThyAds because intact adipocytes are large, buoyant, and fragile, and are therefore poorly captured by droplet-based microfluidic workflow [15-18].

Recent single-nuclei methodologies combining RNA-seq and ATAC-seq have enabled high-resolution mapping of adipose depots, including age-associated pro-inflammatory and metabolic shifts linked to obesity and related pathologies. These technologies have also shown that adipose depots are tailored to their local environment and differ in cellular and molecular composition across the body [14]. For example, subcutaneous and visceral WAT have distinct developmental origins, mechanisms of expansion and disease associations [19]. Additionally, adipocytes remodel over time [20,21]. In humans highly metabolically active brown adipose tissue (BAT), subcutaneous white adipose tissue (WAT), and beige fat, an intermediate form, typically decline with age whereas visceral WAT expands [22-24]. Together, these findings led us to hypothesize that ThyAds are distinct from other adipocyte populations and that their age-associated expansion reflects changes in cellular composition and state.

Here, we used an integrated multiomic strategy to generate the first single-nuclei dataset of ThyAds. By profiling nuclei rather than intact cells, multiomic sequencing overcomes the technical limitations imposed by adipocyte size and fragility. We develop methodologies to efficiently liberate and isolate ThyAds and their nuclei from mouse thymi. By single-nucleus profiling, we identify two highly distinct ThyAd populations, termed ThyAd I and ThyAd II. ThyAd I exhibit a beige fat-like transcriptional program, whereas ThyAd II show features consistent with classic WAT. Notably, ThyAd II-specific accessible chromatin was enriched for consensus sites recognized by Foxn1, the master transcription regulator of TECs. This enrichment suggests a TEC-linked regulatory signature and supports the hypothesis that ThyAd II derive from TECs. Together, our ThyAd multiome resolves two adipocyte programs and provide clues to cellular origin, providing a roadmap to test lineage relationships and functional roles in thymic aging.

RESULTS

ThyAds comprise two discrete subpopulations, one of which has transcriptional hallmarks of beige fat

Thymic adipocytes are technically difficult to recover. We successfully developed an enrichment workflow that combines a retina tissue dissociation protocol and WAT buoyancy-based fractionation, followed by single-nuclei isolation to profile 6-month-old female mice (**Figure 1A**). In mature thymi, scattered multilocular lipid-laden cells are detectable within the subcapsular region, parenchyma, and PVS by ~3 months, while large unilocular white adipocytes become prominent after ~12 months [25]. We therefore reasoned that 6-month-old mice would capture maximal diversity in the ThyAd pool, at a timepoint when thymic output is still preserved but ThyAds are recoverable from a sufficient amount of thymic tissue. After dissection, we extensively cleaned the thymic capsule to minimize contamination while preserving subcapsular and septal ThyAds (**Figure 1B**). Thymi were mechanically and enzymatically digested to generate a single-cell suspension, then fractionated to collect the buoyant adipocyte-enriched layer. Nuclei prepared from the buoyant fraction were robust, with preserved euchromatic and heterochromatic regions and nucleoli (**Figure S1A**).

16 pooled female thymi were used for single-nucleus ATAC-seq plus RNA-seq, yielding 3,610 high-quality nuclei after filtering (**Figure S1B**). Initial uniform manifold approximation and projection (UMAP) clustering indicated substantial hematopoietic carryover, with most nuclei expressing *Ptprc* (*Cd45*) and resolving into expected thymocyte populations based on canonical markers such as *Cd8a*, *Cd4*, *Mki67*, *Hes1* and *Cd5* (**Figure S1C,D**). For example, cluster 8 expressed *Il2ra* but not *Cd8a* or *Cd4*, identifying these cells as DN2/3. Cluster 2 expressed *Cd5* and likely comprised B cells. Cluster 7 expressed *Klrb1c*, which encodes the NK1.1 surface protein. These nuclei are likely derived from iNKT cells. In contrast, signatures of non-hematopoietic thymic stromal populations (TECs, fibroblasts/mesenchyme, endothelium) were minimal or absent. This may reflect either or both a greater abundance of bone marrow-derived cells in the thymus, or a closer apposition of these cells with ThyAds such that they are preferentially carried over with the buoyant fraction following digestion. These data establish a technical framework for ThyAd recovery and set the stage for targeted analysis of the ThyAd compartment.

Two transcriptionally discrete clusters (3 and 10) expressed the canonical adipocyte markers *Pparg* and *Plin1* (**Figure S1C**) as well as *Fabp4* (not shown), consistent with adipocytes. A lipid metabolism gene module further supported adipocyte identity in clusters 3 and 10, whereas cluster 11 (the least abundant cluster) showed weaker and less consistent expression of

126 adipocyte-associated transcripts (**Figure S2A**). We therefore focused on adipocyte clusters 3 and
127 10, yielding 429 high-quality adipocyte nuclei. These nuclei contained a mean of 1533 detected
128 genes and an average depth of 2974 reads per nucleus.

129 We re-clustered adipocyte based on gene expression (RNA-seq UMAP), chromatin
130 accessibility (ATAC-seq UMAP), and a weighted nearest neighbor (WNN) approach that
131 integrates both modalities (**Figure 1C**). This analysis resolved two broad transcriptional programs,
132 termed ThyAd I and ThyAd II, distinguished by differential expression of lipid metabolic genes
133 (**Figure S2B**). A small residual thymocyte cluster expressed *Themis* and *Satb1* (**Figure S3A**) as
134 well as lipid metabolic genes such as *Fasn* (**Figure S2B**) and may reflect doublet nuclei. The
135 remaining clusters lacked thymocyte gene expression and robustly expressed adipocyte markers
136 (e.g., *Pparg*), supporting their adipocyte identity (**Figures S2B** and **S3A**).

137 To define transcriptional states within ThyAds, we identified the top 10 DEGs across
138 clusters. This revealed clear separation between ThyAd transcription programs, with ThyAd I
139 more strongly expressing genes associated with thermogenesis relative to ThyAd II (**Figure S3A**).
140 Restricting analysis to adipocyte nuclei only, we further resolved five distinct ThyAd subclusters–
141 Ia, Ib, IIa, IIb and IIc (**Figure 1D**), consistent with prior evidence showing that ThyAds are
142 morphologically heterogeneous [25].

143 ThyAd Ia nuclei were marked by the expression of Prkar2b and *Fgf14*. In contrast, ThyAd
144 Ib more robustly expressed *Esrrg*, *Ucp1*, and *Cidea* (**Figure 1D**). *Ppara* was also up-regulated in
145 ThyAd Ib (**Table S1**). These genes have been shown to positively regulate beige adipocytes [26-28].
146 These findings strongly suggest that ThyAd I – particularly ThyAd Ib – are beige-like, consistent
147 with work that used imaging to identify UCP1-positive cells detected inside the thymic
148 parenchyma [25]. In contrast, ThyAd II nuclei expressed a distinct program consistent with WAT-
149 like identity (e.g., *Apoe*, **Table S1**) and additional features no observed in ThyAd I. ThyAd IIa was
150 enriched for epithelial-mesenchymal transition (EMT)-associated transcripts including *Prr16* and
151 *Alcam*, while ThyAd IIb/IIc displayed higher levels of *B2m* and *H2-D1* (**Figure 1D**), consistent with
152 increased MHC-I-related gene expression [29]. ThyAd II also expressed *Gpx3*, which has been
153 reported in thymic stromal populations including intermediary fibroblast-like states [30]. Additional
154 feature plots are shown in **Figure S3B**. These results indicate that ThyAd I (in particular ThyAd
155 Ib) resembles beige-like adipocytes, whereas ThyAd II is more WAT-like and exhibits an EMT-
156 /antigen-presentation-associated transcriptional signature.

157 Because ThyAd I and ThyAd II subclusters were readily distinguishable by the
158 thermogenic transcription signature in ThyAd I (**Figure 1D**), we combined the ThyAd Ia+Ib and
159 IIa+IIb+IIc subclusters and performed differential expression analysis (**Table S2**). Gene

160 expression differences between combined ThyAd I and ThyAd II nuclei are shown in **Figure 2A**.
161 For example, *Prdm16* and *Ppara* were significantly enriched in ThyAd I, encoding transcriptional
162 regulators of beige/brown fat [31,32], while Retn and Prr16 were significantly enriched in ThyAd II,
163 encoding WAT-associated protein Prr16 [33] and the adipokine resistin, a regulator of adipogenesis
164 [34], respectively. Gene ontogeny (GO) analysis further supported functional divergence: ThyAd I
165 was enriched for pathways including "Mitochondrial organization" and "Positive regulation of cold-
166 induced thermogenesis", whereas ThyAd II was enriched for "Epithelial mesenchymal transition"
167 (**Figure 2B**).
168
169 **Single-nucleus ATAC-seq identifies state-specific chromatin accessibility and**
170 **transcriptional factor motif enrichment in ThyAds**
171 In addition to improving resolution of ThyAd states, the ATAC-seq component of the multiomic
172 dataset enables inference of regulatory programs by identifying transcriptional factor (TF) motifs
173 enriched in accessible chromatin. Moreover, because the chromatin state can precede or linger
174 relative to active gene expression, the chromatin states can reflect transcription potential as well
175 as recent enhancer decommissioning This can provide information on the possible antecedents
176 for given populations because silent but recently decommissioned genes can retain areas of open
177 chromatin in progeny cells. Because genomic DNA is fully preserved within the nuclei while much
178 of the mRNA is lost, the ATAC-seq portion of the data provides high-quality information on gene
179 expression states in isolated nuclei. We analyzed the ATAC-seq data focusing on genes
180 associated with beige adipocytes: *Ppara*, *Cidea* and *Ucp1*. In all cases, increased chromatin
181 accessibility was highly associated with the ThyAd Ib subcluster (**Figure 3A**). Additional genes
182 are shown as expression and ATAC accessibility feature plots in **Figure S4**.
183 To identify candidate TFs underlying ThyAd state differences, we compared TF motifs
184 enriched in between ThyAd I and ThyAd II. ThyAd I accessible regions were enriched for motifs
185 consistent with adipocyte differentiation and beiging, including EBF, Plagl1, PPAR and Esrrg
186 (**Figure 3B**). In contrast, ThyAd II accessible chromatin was enriched for Foxn1, hypoxia-inducible
187 factor-1 (HIF-1), Wilms tumor protein 1 (WT1), Krüppel-like factor 12 (KLF12), and KLF1 motifs.
188 Notably, Foxn1 is a master transcriptional regulator of thymic epithelial cells [35], suggesting a TEC-
189 linked regulatory imprint in the ThyAd II population. This idea is consistent with lineage tracing
190 experiments which identify Foxn1-expressing cells a progenitors of at least some adipocytes [36].
191 Together with the EMT signature associated with ThyAd II gene expression (**Figure 1D and**
192 **Figure 2B**), these results are consistent with a model in which ThyAd II white adipose cells arise
193 from TECs. Consistent with this interpretation, transcripts encoding *Ebf2*, *Esrrg* and *Plagl1* were

194 detected in subsets of ThyAd nuclei (**Figure S4A**). In contrast, other TFs highlighted by motif
195 enticement (including *Foxn1*) were not detectably expressed yet displayed accessible regulatory
196 regions (**Figure S4A-B**, **Tables S1 and S2**), consistent with residual chromatin accessibility
197 following recent TF activity or enhancer decommissioning. Together, the data show increased
198 accessibility at thermogenic loci and enrichment of EBF, PPAR, and ESRRG motifs in ThyAd I,
199 while ThyAd II is enriched for FOXO1, HIF, and KLF1 motifs, consistent with a distinct and
200 possibly TEC-linked regulatory imprint.
201
202 **Younger (4-month-old) male mice harbor ThyAd I and II populations distinct from gonadal**
203 **fat**
204 We also profiled ThyAds from 4-month-old male mice to align sampling with the earlier kinetics of
205 thymic involution in males compared with females [37-39]. Whereas 6-month-old females provided
206 an optional window to capture ThyAd heterogeneity while thymic output remains relatively
207 preserved, we reasoned that males would reach a comparable stage of remodeling at an earlier
208 age. In mice, the thymus reaches near-maximal size around 5 weeks of age and then declines in
209 cellularity. In male C57BL/6 mice, thymic cellularity decreases by approximately 50% by 4 months
210 [40]. This is matched in human thymic tissue 26-49 years old, where the perivascular space (PVS)
211 comprises 50-60% of the thymic compartment and adipose tissue is easily identified [2]. We
212 therefore selected 4 months in males as a practical and biological window to capture ThyAds
213 during an early-to-intermediate phase of involution.
214 We isolated ThyAd nuclei from 6 male mice maintained on standard chow and profiled
215 them by single-nucleus RNAseq. From the same animals, we also collected gonadal (epididymal)
216 white adipose tissue (gWAT) as a visceral fat comparator (**Figure 4A**). As in the female dataset,
217 *Ptprc*+ nuclei carried through purification were manually removed prior to clustering. Joint
218 clustering of ThyAd and gWAT nuclei revealed that the thymic and gonadal adipocyte
219 transcriptomes were largely distinct, with ThyAd nuclei again segregating into two discrete
220 clusters which neighbored but were distinct from specific gWAT populations (**Figure 4B**, gWAT II
221 and III). Another gWAT cluster (**Figure 4B**, gWAT Ia/b). A rare thymic cluster expressed *Esrrg*,
222 *Ppara* and *Ppargc1b*, consistent with a ThyAd I (beige-like) program (**Figure S5A**). In contrast,
223 the ThyAd II cluster more closely aligned with one of the gWAT clusters, suggesting a more WAT-
224 like transcriptional state (**Figure 4B** and **Figure S5A**). Feature plots confirmed strong expression
225 of *Ppara* and *Esrrg* in ThyAd I (**Figure 4B-C**). These nuclei were also enriched for *Cidea* and *Ghr*
226 (**Figure S5B**). When clustering thymic nuclei alone, ThyAd I and II remained clearly separable,
227 marked for example by *Ppara* and *Ghr* (growth hormone receptor, **Figure 4D**). The most

228 differentially expressed ThyAd I gene was *Ppara*, whereas ThyAd II was enriched for *Xdh*, *Fabp4*,
229 *Adgrl4*, *Klf12* and *Tgfb2* (**Table S3**). Notably, *Tgfb2* (TGFβ2) has been implicated in promoting
230 thymic involution [41]. Although the different ThyAd clusters grouped more closely to gWAT clusters
231 than to one another, we also assessed gene expression differences between the two tissues by
232 grouping clusters and normalizing their gene expression. Among genes expressed in >5% of one
233 or both nuclei with Adj. $p < 0.05$ and fold change >4 (529 genes), beige/brown adipocyte
234 signatures were again a dominant program in ThyAds, as highlighted by enrichment of *Esrrg*,
235 *Ppara*, *Ppargc1b* and *Cidea* in ThyAd nuclei (**Table S4**). Other genes globally enriched in ThyAds
236 compared to gWAT included *Themis*, *Robo2*, *Dll4* and *Rasal2*. In contrast, gWAT-enriched genes
237 included *Retn*, *Gpx1*, *Cfd*, *Lep* and *Apoe*. Both populations expressed core adipocyte genes
238 including *Pparg* (**Figure 4D**) and *Cd36* (not shown).
239
240 **UCP1$^+$ cells largely localize within the subcapsular cortical thymic compartment, whereas**
241 **lipid-rich unilocular adipocytes localize to septa and perivascular space**
242 Epicardial/perithymic fat is heterogenous, with some beige-like cells strongly expressing UCP1,
243 a key enzyme that enables energetic equivalents to be consumed, indirectly generating heat [42].
244 Although thymi used for sequencing were obtained from mice younger than 6 months old and
245 were extensively cleaned of extrathymic fat prior to processing (**Figure 1B**), it remained formally
246 possible that the beige-like ThyAd I signal reflected residual contamination outside the capsule.
247 Prior work, however, has identified UCP1$^+$ cells within the thymic parenchyma [25]. To directly
248 assess localization, we performed Immunofluorescence on 6-month-old female thymi. For this
249 experiment, thymi were intentionally not cleaned of extrathymic fat, enabling direct comparison of
250 perithymic adipose tissue with intrathymic UCP1$^+$ cells.
251 As expected [42], perithymic fat and connective tissue abutting the thymic capsule was
252 heterogenous, with regions containing large unilocular lipid droplets and others containing
253 densely packed multilocular, BAT-like adipocytes with strong UCP1 staining. In contrast, UCP1$^+$
254 cells within the thymic parenchyma were sparse and exhibited weaker, punctate UCP1. Omission
255 of the primary antibody eliminated both the intra- and extrathymic UCP1 signal (**Figure 5**). In
256 parallel, PPARγ antibody staining and BODIPY labeling highlighted adipocytes with large
257 unilocular lipid droplets enriched within thymic septa and the capsule border, consistent with
258 ThyAd II (**Figure S6**). Together, these data support the presence of beige-like ThyAd I cells within
259 the thymic capsule and argue against perithymic contamination as the primary source of the
260 ThyAd I transcriptional program detected by multiomic sequencing.

261 **DISCUSSION**

262 Recent advances in single-nuclei methodologies combining RNA-seq and ATAC-seq have been
263 used to investigate the heterogeneity of adipose tissue depots throughout the body [14,43].
264 Separately, they have been used to profile thymocytes and thymic stromal cells [15-18]. However,
265 adipocytes associated with the thymus (ThyAds) remain uncharacterized at a molecular level.
266 Here, we developed methodologies to liberate and isolate adipocyte and their nuclei from mouse
267 thymi, generating the first single-nuclei datasets of ThyAds. We identify similarities and
268 differences in transcriptional profiles compared to a peripheral adipose depot. We profile nuclei
269 from female and male thymi at two different ages, providing the first single-nucleus ThyAd atlas
270 and expanding our understanding of ThyAds and their potential roles in the thymus and during
271 thymic involution. By single-nucleus profiling, we identified two distinct ThyAd populations, termed
272 ThyAd I and ThyAd II.

273 snRNAseq revealed that ThyAds express mature adipocyte-associated markers such as
274 *Pparg*, *Fabp4*, and *Plin1*. No thymic preadipocytes were identified based on co-expression of
275 markers such as *Pdgfra/b*, *Pref1* and *Cd34* [44]. This is likely due to their relative lack of buoyancy.
276 These studies also revealed a population of ThyAds expressing a highly metabolically active
277 transcription program similar to beige adipose cells, termed 'ThyAd Ib'. These nuclei were
278 differentiated by significant expression of *Ucp1*, *Ppara* and *Esrrg*. , hallmarks of beige and brown
279 adipocytes. *Esrrg* for example encodes an orphan nuclear receptor expressed in metabolically
280 active tissues (e.g., brain, heart, skeletal muscle, BAT) that promotes adipocyte beiging by
281 activating mitochondrial biogenesis and oxidative metabolism [27]. *Ppara* encodes a nuclear
282 receptor associated with metabolically active tissues such as heart and brown adipose tissue
283 (BAT) that oxidize fatty acids at a high rate [45]. *Ppara* is also expressed in hepatocytes, where it
284 promotes fatty acid oxidation and ketogenesis during fasting [46,47]. In combination with PPARγ,
285 PPARα can induce beiging of white adipose tissue [48]. *Cidea*, which can be induced by the
286 combined expression of PPARγ and PPARα and encodes a transcription coregulator that
287 activates *Ucp1* expression [28]. *Prdm16* and *Ucp1* expression are also hallmarks of BAT [31].
288 PRDM16 represses type-1 interferon signaling in adipocytes which promotes thermogenic
289 programming [49]. Interestingly however, these nuclei did not strongly express other genes
290 associated with beige adipocyte gene expression programs, e.g. *Tbx1*, *Shox2*, *Tmem26*, or
291 *Hoxc9*, indicating that ThyAd Ib may be distinct from previously defined populations of beige
292 adipocytes. An intermediate population – 'ThyAd Ia' – shared expression of beige/brown genes
293 with ThyAd Ib such as *Ppara* and *Prdm16* but with little expression of *Ucp1*. DEG analysis of

294 ThyAd clusters alone identified *Acsl1*, *Prkr2b* and *Mecom* among the topmost ThyAd Ia-enriched
295 genes. The products of these genes are known to positively regulate adipogenesis and FA
296 metabolism within BAT [50-52]. ThyAd IIs displayed differential expression of genes such as
297 *Col15a1*, *Prr16*, and *Pbx1*. These genes are often associated with EMT and ECM remodeling [53-
298 56]. EMT has been associated with more plastic and stem-like states, allowing de-differentiation
299 and developmental plasticity, including the ability to transition to adipocytes [57]. Within the thymus,
300 age-associated TECs (aaTECs) are also associated with limited EMT signatures [30].

301 Analysis of transcription factor motifs enriched in open ThyAd chromatin supports the
302 finding of two broad transcriptional ThyAd I and II programs and identifies potential regulators that
303 may differentially regulate the two populations. Motif sequences for Esrrg, Ebf2 and Nr4a2 were
304 highly enriched in ThyAd I, consistent with their significant expression in this population and roles
305 in maintaining a beige-like transcription profile [14,27,58,59]. Both Ebf2 and Esrrg have been
306 demonstrated to promote and maintain a beige/brown transcriptional program [27,60,61]. Esrrg
307 accessibility was mostly restricted to ThyAd Ib in both male and female mice, suggesting Esrrg
308 plays an important role in ThyAd Ib's beige-like transcriptional state. Though *Ebf2* was expressed
309 highly in all clusters, chromatin accessibility displayed a gradient pattern with higher accessibility
310 in ThyAd Is and lower accessibility in ThyAd IIs. Interestingly, though Plagl1 motif accessibility
311 was enriched in ThyAd Is, its expression by RNAseq was increased in ThyAd IIs.

312 ThyAd IIs instead showed increased accessibility for WT1, KLF12, and KLF1. WT1 is
313 known to negatively regulate thermogenic gene expression and beige fat identity [62]. WT1 also
314 modulates EMT/MET during development [63,64]. Interestingly, ThyAd II showed the strongest
315 enrichment for Foxn1 motifs, which were not detected within the RNAseq. This is consistent with
316 a model in which Foxn1 may have been expressed earlier in the etiology of ThyAd II. The origin
317 of adipocytes within the thymic compartment is not well understood. Adipogenesis involves
318 several tightly regulated steps, including the upregulation of PPARγ, a transcriptional factor
319 required for activation of downstream genes [65]. Aire-expressing TECs can give rise to "mimetic"
320 cells that adopt characteristics of peripheral cells including antigens that would not otherwise be
321 found in the thymus. These cells aid in thymic selection and the generation of central tolerance
322 [66]. In humans, Aire deficiency has been associated with Plin-1 autoreactivity and autoimmune
323 adipose infiltration [67,68]. Prior work has identified adipogenic potential in the thymic SVF [36]. These
324 findings suggest that at least a subset of the identified ThyAds may represent an uncharacterized
325 depot of mimetic cells that eluded identification due to their buoyancy. Within the thymus,
326 adipocytes have been suggested to arise from multiple sources, such as infiltration via proximity

327 to the PVS or transdifferentiation from stromal cells with adipogenic potential [69,70]. Lineage tracing
328 experiments using LacZ reporters indicate that at least some adipocytes are derived from Foxn1-
329 expressing TECs [36]. We found that differentially open chromatin in WAT-like ThyAd II nuclei are
330 enriched in binding sites for Foxn1, suggesting that this specific population may emerge from
331 TECs. Other populations Foxn1-negative, EpCAM-negative stromal cells have been identified
332 with adipogenic potential [71]. Together with our findings of multiple distinct ThyAd populations,
333 these findings are most consistent with a complex etiology for ThyAds.
334 We used confocal imaging to identify UCP1+ cells within the thymic parenchyma. These
335 cells were sparse and well-spaced and mostly confined to cortical regions. These findings are
336 consistent with work from Langhi et al., who identified several lipid-laden, Plin1+ populations
337 including preadipocytes, brown adipocytes (UCP1+), macrophages (Iba1+), and pericytes (Ng2+)
338 within the thymic parenchyma, surrounding blood vessels, and the subcapsular zone [25].
339 Thymocyte maturation is dependent on cellular crosstalk within the thymic
340 microenvironment, including between thymic stromal cells and thymocytes. For example, TECs
341 and fibroblasts secrete factors (e.g., IL-7, SCF, DLL4) that drive thymocyte
342 proliferation/differentiation [72]. Reciprocally, thymocytes provide TEC differentiation signals (e.g.,
343 RANKL, CD40, LTβ) to maintain thymic architecture [1]. TEC-derived cells in the thymus are known
344 to play additional roles beyond antigen presentation [73]. More work is required to define ThyAd
345 functions in antigen presentation and other functions such as providing trophic or metabolic
346 support to thymocytes or TECs. Similarly, although ThyAds expand with age their role in thymic
347 involution remains incompletely understood. Injection of T cell progenitors from young mice into
348 aged thymi fails to rescue declining thymopoiesis. Conversely, transplantation of fetal thymic
349 lobes into 18-month-old RAG1$^{-/-}$ mice restores host thymocyte counts to that of 6-8 week-old mice
350 [74]. The fact that other strategies, such as injection of fetal TECs or ectopic expression of Foxn1
351 within adult TECs, only partially rescues aged thymi indicates that multiple attributes intrinsic to
352 aged thymi are responsible for loss of T cell output [75-77]. The possible contribution of one of more
353 ThyAd subsets to this process also awaits experimentation.
354
355 **Limitations of the study**
356 Our findings identify heterogeneity in ThyAds and identify beige-like cells expressing UCP1 within
357 the thymic parenchyma. Although we confined the study to relatively young mice to reduce
358 accumulation of epicardial/perithymic fat which could confound the study, and although thymi
359 were extensively cleaned of fat outside the capsule before processing, it remains formally possible
360 that one or more of the ThyAd subclusters could reflect contamination from perithymic fat, which

361 is known to harbor beige-like cells. It is also possible that one or more subclusters could be
362 molecularly indistinguishable from perithymic fat. Although prior lineage tracing work pinpoints
363 TECs as a source for at least some ThyAds, and although our work is consistent with a TEC origin
364 for ThyAd II, this has not been formally demonstrated. Finally, the study is intended to provide the
365 first molecular ThyAd atlas, and as such contains no information of the functions for these cells in
366 T cell development or thymic involution.

367 **METHOD DETAILS**

368 **Laboratory mice**

369 All mice were C57BL/6J background (#000664, Jackson Laboratories, Bar Harbor, Maine, USA).
370 Mice were housed on a 12h dark/light cycle in groups (maximum five mice per cage) with ad
371 libitum access to water and standard chow diet. All procedures were performed in accordance
372 with the University of Utah Institutional Animal Care and Use Committee (Protocol #00001553).
373

374 **ThyAd isolation**

375 Intact thymi were quickly removed and transferred to a petri dish on ice with ~300uL PBS to keep
376 tissue moist. Thymic capsules were cleaned of directly attached perithymic fat and connective
377 tissues, rinsed a final time with PBS, and transferred to a 15mL conical tube. Digestion Buffer
378 (1mM CaCl2, 250mM sucrose, 1.5mM MgCl2, 10mM KCl, 15mM HEPES, 0.1% BSA) with DNase
379 I (8 μg/mL, D513, Sigma Aldrich) and Collagenase II (2 mg/mL, C1764, Sigma Aldrich) in DMEM-
380 F12 10% FBS was added to each sample and thymi were digested for approximately 10-15
381 minutes at 37°C, horizontally on a shaker set at 300 rpm. Once most of the thymic tissue was
382 digested, an equal volume of FBS was added to each sample to quench the reaction, mixed by
383 gentle pipetting. Samples were fractionated by an initial centrifugation at 300 × *g* at 4°C. The
384 topmost white layer containing mature, floating adipocytes was transferred to a clean 15 mL tube
385 (Figure 1). Then, 10 mL of Wash Buffer (DMEM-F12, 15mM HEPES, 10% FBS) were added to
386 each sample and mixed by gentle inversion and/or trituration with a micropipette to prevent
387 bursting of the adipocytes. Samples were left on ice for 10 min, followed by a second round of
388 centrifugation at 150 × *g* at 4°C. The white floating layer was transferred to a 5 mL conical tube
389 and washed with 4 mL Wash Buffer. Samples were left on ice for 10 min, and spun at 150 × *g* at
390 4°C. The floating fraction was collected and transferred to a clean 1.5 mL eppendorf tube. Without
391 adding more media, samples were centrifuged at 150 *x g* at 4°C. Residual buffer was carefully
392 removed from the bottom of the tube with a 5 mL syringe and 21-gage needle. The remaining
393 white layer of packed adipocytes was transferred to a clean, prechilled 1.5 mL eppendorf tube for
394 nuclei isolation. For the data shown in Figure 4, 6 male thymi were collected, combined, and
395 processed similarly. Gonadal (inguinal) fat (gWAT) was prepared from the same mice in parallel
396 as a quality control.
397

398 **Nuclei and 10X library preparation**

399 To isolate nuclei, samples were incubated with 100 μL 0.1x lysis buffer for 3-5 min on ice as
400 previously described (10X Genomics, Demonstrated Protocol CG000366 Rev D). After washing
401 and centrifugation following the outlined protocol, nuclei were resuspended in diluted 1x Nuclei
402 Buffer (10X Genomics, PN 2000207). The concentration of nuclei was determined by AO/PI using
403 a Luna-FL (Logos Biosystems, Inc., Gyeonggi-do, Korea). Approximately 5,000 nuclei were
404 immediately loaded onto a 10X Next GEM Chip J (10X Genomics, PN 1000230). Single-nuclei
405 libraries were prepared using Chromium Next GEM Single Cell Multiome Reagent Kit A reagents
406 (10X Genomics, PN 1000284) and assessed for quality using an Agilent D1000 ScreenTape.
407 Libraries were sequenced on an Illumina NovaSeq X instrument targeting 100 million paired end
408 reads (GEX) and 300 million paired end reads (ATAC) of 150 bp for each sample.
409
410 **Data analysis**
411 For female thymi, reads were aligned to the *mm10* reference genome (package 2020-A) to
412 generate feature-barcode matrices using cellranger (version 2.0.2). Analysis was performed as
413 described in the Seurat WNN and Signac 10x multiomic analysis vignettes [78,79]. Briefly, doublets
414 with high feature count and low-quality nuclei were removed by applying thresholding filters for
415 number of ATAC transcripts (nCount_ATAC >500 & <70,000), unique genes (nFeature_RNA
416 >200 & <2,500), mitochondrial mRNA content (mt.percent_RNA <20%), nucleosome signal (<2),
417 and TSS enrichment (>1). 3,610 nuclei were recovered using this method for downstream
418 analysis (S1B). Utilizing the Seurat SCTransform pipeline, dimensional reduction (PCA) was
419 performed on the top 3,000 most variable genes. Equivalent normalization of the ATACseq data
420 was performed by latent semantic indexing (LSI). A 'weighted nearest neighbor' (WNN) UMAP
421 was generated using the FindMultiModalNeighbors function, taking both RNAseq and ATACseq
422 datasets into account for subsequent UMAP and cluster visualization. Ptprc-enriched clusters
423 were identified and excluded from downstream analyses while ThyAds were identified by
424 enrichment of adipocyte markers Pparg and Plin1 but lack of residual immune cell markers such
425 as CD8, CD4, and Ptprc (S1C, S1D). 429 remaining adipocytes were reclustered using the
426 SCTransform pipeline.
427 For male thymi, 4,342 thymic and 4,968 gWAT nuclei were identified in each sample, respectively.
428 Following removal of Ptprc-expressing cells, 1,521 filtered ThyAd nuclei and 3,806 filtered gWAT
429 nuclei were present. Individual samples were normalized by SCTransform using the top 2,000
430 most variable genes followed by exclusion of immune cells as described above. Adipocyte
431 clusters from individual samples were subjected to SCTransform and then merged by applying

432 the Merge() and IntegrateLayers() functions. Merged dataset UMAPs were then generated as
433 above by applying FindNeighbors() and FindClusters() with the standard pipeline. Subsequent
434 filtering of adipocytes and removal of residual immune cells was performed as described above.
435 After subsetting of adipocytes, SCTransform() was reapplied to normalize and scale expression
436 of merged samples. Defining markers were again determined by applying the FindAllMarkers or
437 FindMarkers function to identify differentially enriched genes in each cluster. Both datasets are
438 hosted on the Gene Expression Omnibus (GEO) server under accession ID GSE319467. Cluster-
439 defining markers were determined by applying the FindAllMarkers or FindMarkers function, which
440 use a non-parametric Wilcoxon rank sum test with Bonferroni correction on all normalized
441 features. For applicable figures, cluster-enriched markers are reported as levels of significance
442 denoted by *$p < 0.05$, **$p < 0.01$, ***$p < 0.001$, and ****$p < 0.0001$. We also compared combined
443 ThyAD clusters against all gWAT clusters to identify differentially expressed genes by applying
444 FindMarkers(). Gene expression was normalized for comparison between tissues using
445 SCTransform(). Filtered genes had an average log2FC > 2 or < -2, and Adj. $p \leq 0.05$.
446
447 **Motif, transcription factor, and GO analysis**
448 Motif analysis was performed using chromVAR and additional packages as outlined in the Signac
449 motif analysis and Seurat WNN vignettes [79]. Clusters were compared against each other to
450 identify the topmost differentially accessible motifs (p.val <0.05). To identify transcription factors
451 (TFs) which may underlie ThyAd cluster transcriptional state, TFs with both high differential
452 expression and their corresponding accessible motifs were determined using Seurat's 'presto'
453 package, which uses a Wilcox rank sum test to calculate p-values for both datasets and returning
454 only TFs with p.val <0.01. GO analysis was performed on ThyAd I and ThyAd II cluster DEGs
455 with adjusted p.val <0.05 using the 'fgsea' R package for Biological Process and Hallmark gene
456 sets [80].
457
458 **Immunofluorescence and confocal microscopy**
459 6-month old mice were euthanized by isofluorane and perfused with PBS. Intact thymi and directly
460 attached connective tissue were carefully removed, washed in PBS, and postfixed for 30 min in
461 4% (w/v) paraformaldehyde (PFA). After 3x PBS washes for 20 min each, thymi were incubated
462 in 10% sucrose for 1 hr and then left in 20% sucrose overnight at 4°C. The following day, thymi
463 were incubated in a series of 30% sucrose for at least 2 hr, then incubated in 2:1 OCT
464 compound:20% sucrose for 1 hr. Tissue was embedded in 100% OCT over a dry ice and 2-

465 propanol slurry for sectioning. 10-20 μm cryosections were dried for 40-60 min at 37°C and
466 rehydrated in cold PBS. Tissue was rinsed 3x in PBST (0.1% Tween 20), and permeabilized in
467 PBST for 15 min. Detergent was removed by rinsing 3x in PBS, following which samples were
468 incubated in prewarmed 0.5-1X TrueBlack Lipofluscin Autofluorescence Quencher (Biotium,
469 Fremont, CA) for 2 min. Slides were blocked for 1 hr at RT in PBS containing 10% normal donkey
470 serum, 5% BSA, and 0.2% Triton-X, and incubated overnight in a primary antibody cocktail (10%
471 donkey normal serum, 5% BSA) containing rabbit anti-UCP1 or rabbit anti-PPARγ (Cell Signaling
472 Technologies, MA, USA) at 4°C. Sections were washed in PBS for 20 min thrice, followed by a 2
473 hr incubation with a secondary buffer cocktail at RT (1% BSA, 1:2000 Hoescht 33342, Thermo
474 Fischer Scientific H3570) with or without donkey anti-Alexa Fluor 647 nm (1:400, Invitrogen, La
475 Jolla, CA, USA). Slides were washed and mounted with Fluoromount-G (Thermo Fischer
476 Scientific 00-4958). If substantial TrueBlack was removed from slides after incubation with
477 blocking buffer, the post-staining treatment protocol was used per manufacturer's protocol.
478 Stained sections were imaged by resonance scanning confocal microscopy (A1R confocal system
479 and Eclipse Ti inverted microscope; Nikon, Melville, NY, USA) with a 20X objective and 3X or 8X
480 optical zoom (0.41μm/px).

481 **AUTHOR CONTRIBUTIONS**

482 N.J.S. and D.T. conceived the study. KEV helped with generation of the ThyAd isolation protocol.
483 N.J.S. and A.F. performed experiments. N.J.S. analyzed the data and generated figures. All
484 authors contributed to the writing of the manuscript.

485

486 **ACKNOWLEDGEMENTS**

487 We thank W.-L. Lo for critical reading of the manuscript. We thank M. Chandrasekharan for help
488 with graphics. We thank B. Dalley, O. Allen and the University of Utah Huntsman Cancer Institute
489 High-Throughput Genomics Core Facility. This work was supported by awards from the University
490 of Utah Center Diabetes and Metabolism Research Center (DMRC), the NIH/NIAID
491 (R01AI162929) and the Praespero Autoimmune Foundation (Canada) to D.T.

492

493 **DECLARATION OF INTERESTS**

494 The authors declare no competing interests.

495 **FIGURE LEGENDS**

496 **Figure 1. Female ThyAds are heterogeneous, with one subclustered harboring**
497 **transcriptional signatures of metabolically active beige fat.**

498 (A) Experimental design for isolation and multiomic sequencing of murine ThyAds. Thymi were
499 processed by mechanical disaggregation, digestion, centrifugation (isolation by buoyancy) and
500 nuclei isolation prior to single-nucleus ATACseq + RNAseq multiomics.

501 (B) Example thymus prior to and after removal of perithymic fat. The septa and thymic lobes were
502 kept intact such that the fatty tissue between the lobes is retained.

503 (C) UMAP projection and clustering of ThyAds by RNAseq, ATACseq, and Weighted Next
504 Neighbor (WNN) analysis. ThyAds (n = 429, avg gene count 2,974) were reclustered after removal
505 of Prprc-expressing nuclei. A residual Ptprc+ cluster was also present.

506 (D) Expression of most distinguishing ThyAd marker genes by cluster. A heatmap displaying the
507 top 10 DEGs within each ThyAd subpopulation is shown.

508

509 **Figure 2. ThyAd I and II display highly differential gene expression.**

510 (A) Violin plots highlighting differential and shared expression of ThyAd I and II cluster-defining
511 genes. Recolored UMAP denotes superclusters Ia/b and Ia/b/c are shown at right.

512 (B) GO Biological Process Analysis for ThyAd Is and II superclusters.

513

514 **Figure 3. Differentially accessible chromatin and transcription factor motif enrichment in**
515 **different ThyAd subpopulations.**

516 (A) Single-nucleus ATAC-seq open chromatin genome tracks at the *Ppara*, *Cidea* and *Ucp1* loci
517 are shown for each subpopulation.

518 (B) Motif analysis comparing combined ThyAd I and II subpopulations. The top 6 most enriched
519 motifs are shown for each grouped population. Asterisks denote motifs unique to that population.

520

521 **Figure 4. Male murine ThyAds are heterogenous and transcriptionally distinct from gWAT.**

522 (A) Experimental design for isolation and multiomic sequencing of murine ThyAds.

523 (B) Single-nucleus RNA-seq UMAPs comparing ThyAds with gWAT isolated from 4-month-old
524 male mice. Nuclei were labeled by tissue.

525 (C) Feature plots showing expression of selected marker genes *Ptprc*, *Pparg*, *Fabp4*, *Adipoq*,
526 *Ppara*, and *Esrrg*.

527 (D) ThyAds were reclustered alone to distinguish 1a, Ib, IIa, IIb, and IIc populations. UMAP feature
528 plots are shown for *Ppara*, *Ghr*, *Ppargc1b*, *Pparg*, *Fabp4*, *Fgf14*, and *Esrrg*.
529
530 **Figure 5. UCP1^{+} cells are detectable in the thymic cortical regions of 6-month-old female**
531 **mice.**
532 (A) Top: 0.8 μm confocal Z-stack images of UCP1 immunofluorescence-stained cryosections of
533 a region of a 6-month-old female murine thymus where the cortex meets the capsule. Slides were
534 counterstained with Hoescht. Dense nuclear stain (blue) denotes the thymic parenchyma,
535 predominantly TECs and thymocytes. Intense UCP1 staining is present in perithymic fat attached
536 to the thymic capsule with a distinct expression pattern compared to scattered parenchymal
537 UCP1+ cells (highlighted with yellow arrows). At right is shown a higher magnification image of
538 the same slide. Bottom: an adjacent cryosection stained and imaged identically except lacking
539 the primary antibody.
540 (B) Similarly processed images of a different section from the same thymus.
541
542 **SUPPLEMENTAL FIGURE LEGENDS**
543 **Supplemental Figure 1. Quality control for single-nucleus ATAC-seq plus RNA-seq**
544 **multiomics.**
545 (A) example nuclei following isolation. Areas of heterochromatin are preserved.
546 (B) Thresholding and quality control parameters employed to eliminate low-quality nuclei. Left:
547 mitochondrial regression/normalization. Removed nuclei are shown in gray (top left). Right:
548 Density plot showing retained nuclei by TSS enrichment and total peak fragments. nCount_ATAC
549 quantiles are: 5% 6438.45; 10% 7834; 90% 29520.1. TSS. Enrichment quantiles are: 5% 5.47;
550 10% 5.8; 95% 8.96.
551 (C) WNN UMAP clustering of 3,610 nuclei isolated from the floating fraction of female 6-month
552 old thymic tissue. Clusters 3 and 10 are highlighted (red circles) and identified as Ptprc^{lo} and
553 Pparg^{+}Plin1^{+}. This subset was used for further downstream analysis.
554 (D) Selected marker genes used to identify immune populations and adipocytes are shown as
555 violin plots by cluster.
556
557 **Supplemental Figure 2. Lipid-metabolism-related gene expression comparing whole**
558 **sample and ThyAds.**

559 (A) Dot Plots of whole sample ThyAds showing expression of genes associated with lipid
560 metabolism. Genes associated with lipogenesis (*Fasn*, *Acaca*, *Elovl6*, *Dgat1*, *Dgat2*, *Srebf1*, *Acly*,
561 *Scd1*, *Scd1*) and lipolysis (*Lipe*, *Pnpla2*, *Mgll*, *Gk*, *Abhd5*) are shown.
562 (B) The same analysis was performed for subsetted Pparg+Fabp4+Plin1+ ThyAds and the
563 residual Ptprc+ cluster.
564
565 **Supplemental Figure 3. Expression of selected markers by ThyAds and top DEGs by**
566 **cluster.**
567 (A) Heatmap displaying the top 10 DEGs for cluster including the Ptprc+ nuclei.
568 (B) WNN UMAP projections of genes encoding selected adipokines (*Adipoq*, *Retn*, *Lep*, *Cfd*) and
569 beige/brown adipocyte marker genes (*Cidea*, *Prdm16*, *Ucp1*, *Esrrg*, *Ppargc1a*, *Ppargc1b*). *Plin1*,
570 *Fasn*, *Ebf2*, *Zfp423*, *Col15a1*, *Aldh1a1*, *Prr16* and *Rems3* are also shown.
571
572 **Supplemental Figure 4. Gene expression and open chromatin states of potential ThyAd**
573 **transcription regulators.**
574 (A) Feature plots of WNN UMAPS showing expression and chromatin accessibility for additional
575 genes. *Ebf2*, *Esrrg*, *Plagl1*, and *Foxn1* are shown. Gene expression plots for *Foxn1* could not be
576 generated because Foxn1 was not expressed in any nucleus. The WNN plot from Figure 1C is
577 recapitulated at right for comparison.
578 (B) Single-nucleus ATAC-seq open chromatin genome tracks at the *Foxn1* locus is shown for
579 each subpopulation.
580
581 **Supplemental Figure 5. Gene expression differences associated with ThyAd and gWAT**
582 **tissue from 4-month-old male mice.**
583 (A) Heatmap displaying the top 10 DEGs within each ThyAd and gWAT subpopulation is shown.
584 (B) Similar to Figure 4C except additional genes are shown: *Ebf2*, *Cidea*, *Prdm16*, *Ghr*, *Ebf1*, and
585 *Aifm2*.
586
587 **Supplemental Figure 6. PPARγ-positive cells identified within the thymus.**
588 IF image of a 16 μm cryosection of a thymus from a 6-month-old female mouse. Samples was
589 stained with BODIPY (488 nm), rabbit anti-PPARγ (647 nm) and Hoescht (405 nm). Dashed lines
590 highlight demarcation between thymic parenchyma and capsule or septa.

591 **REFERENCES**

592

593 1. Li, Y.R., and Zuniga-Pflucker, J.C. (2023). Thymus aging and immune reconstitution,
594 progresses and challenges. Semin Immunol *70*, 101837. 10.1016/j.smim.2023.101837.
595 2. Flores, K.G., Li, J., Sempowski, G.D., Haynes, B.F., and Hale, L.P. (1999). Analysis of
596 the human thymic perivascular space during aging. J Clin Invest *104*, 1031-1039.
597 10.1172/JCI7558.
598 3. Lynch, H.E., Goldberg, G.L., Chidgey, A., Van den Brink, M.R., Boyd, R., and
599 Sempowski, G.D. (2009). Thymic involution and immune reconstitution. Trends Immunol
600 *30*, 366-373. 10.1016/j.it.2009.04.003.
601 4. Min, H., Montecino-Rodriguez, E., and Dorshkind, K. (2004). Reduction in the
602 developmental potential of intrathymic T cell progenitors with age. J Immunol *173*, 245-
603 250. 10.4049/jimmunol.173.1.245.
604 5. Aw, D., Silva, A.B., Maddick, M., von Zglinicki, T., and Palmer, D.B. (2008). Architectural
605 changes in the thymus of aging mice. Aging Cell *7*, 158-167. 10.1111/j.1474-
606 9726.2007.00365.x.
607 6. Cisneros, B., Garcia-Aguirre, I., Unzueta, J., Arrieta-Cruz, I., Gonzalez-Morales, O.,
608 Dominguez-Larrieta, J.M., Tamez-Gonzalez, A., Leyva-Gomez, G., and Magana, J.J.
609 (2022). Immune system modulation in aging: Molecular mechanisms and therapeutic
610 targets. Front Immunol *13*, 1059173. 10.3389/fimmu.2022.1059173.
611 7. Weng, N.P., Akbar, A.N., and Goronzy, J. (2009). CD28(-) T cells: their role in the age-
612 associated decline of immune function. Trends Immunol *30*, 306-312.
613 10.1016/j.it.2009.03.013.
614 8. Saurwein-Teissl, M., Lung, T.L., Marx, F., Gschosser, C., Asch, E., Blasko, I., Parson,
615 W., Bock, G., Schonitzer, D., Trannoy, E., and Grubeck-Loebenstein, B. (2002). Lack of
616 antibody production following immunization in old age: association with CD8(+)CD28(-) T
617 cell clonal expansions and an imbalance in the production of Th1 and Th2 cytokines. J
618 Immunol *168*, 5893-5899. 10.4049/jimmunol.168.11.5893.
619 9. Dorshkind, K., and Swain, S. (2009). Age-associated declines in immune system
620 development and function: causes, consequences, and reversal. Curr Opin Immunol *21*,
621 404-407. 10.1016/j.coi.2009.07.001.
622 10. Youm, Y.H., Yang, H., Amin, R., Smith, S.R., Leff, T., and Dixit, V.D. (2010).
623 Thiazolidinedione treatment and constitutive-PPARgamma activation induces ectopic
624 adipogenesis and promotes age-related thymic involution. Aging Cell *9*, 478-489.
625 10.1111/j.1474-9726.2010.00574.x.
626 11. Laan, M., Haljasorg, U., Kisand, K., Salumets, A., and Peterson, P. (2016). Pregnancy-
627 induced thymic involution is associated with suppression of chemokines essential for T-
628 lymphoid progenitor homing. Eur J Immunol *46*, 2008-2017. 10.1002/eji.201646309.
629 12. Billard, M.J., Gruver, A.L., and Sempowski, G.D. (2011). Acute endotoxin-induced
630 thymic atrophy is characterized by intrathymic inflammatory and wound healing
631 responses. PLoS One *6*, e17940. 10.1371/journal.pone.0017940.
632 13. Howard, J.K., Lord, G.M., Matarese, G., Vendetti, S., Ghatei, M.A., Ritter, M.A., Lechler,
633 R.I., and Bloom, S.R. (1999). Leptin protects mice from starvation-induced lymphoid
634 atrophy and increases thymic cellularity in ob/ob mice. J Clin Invest *104*, 1051-1059.
635 10.1172/JCI6762.
636 14. Emont, M.P., Jacobs, C., Essene, A.L., Pant, D., Tenen, D., Colleluori, G., Di Vincenzo,
637 A., Jorgensen, A.M., Dashti, H., Stefek, A., et al. (2022). A single-cell atlas of human and
638 mouse white adipose tissue. Nature *603*, 926-933. 10.1038/s41586-022-04518-2.

15. Bautista, J.L., Cramer, N.T., Miller, C.N., Chavez, J., Berrios, D.I., Byrnes, L.E., Germino, J., Ntranos, V., Sneddon, J.B., Burt, T.D., et al. (2021). Single-cell transcriptional profiling of human thymic stroma uncovers novel cellular heterogeneity in the thymic medulla. Nat Commun *12*, 1096. 10.1038/s41467-021-21346-6.
16. Cordes, M., Cante-Barrett, K., van den Akker, E.B., Moretti, F.A., Kielbasa, S.M., Vloemans, S.A., Garcia-Perez, L., Teodosio, C., van Dongen, J.J.M., Pike-Overzet, K., et al. (2022). Single-cell immune profiling reveals thymus-seeding populations, T cell commitment, and multilineage development in the human thymus. Sci Immunol *7*, eade0182. 10.1126/sciimmunol.ade0182.
17. Lavaert, M., Liang, K.L., Vandamme, N., Park, J.E., Roels, J., Kowalczyk, M.S., Li, B., Ashenberg, O., Tabaka, M., Dionne, D., et al. (2020). Integrated scRNA-Seq Identifies Human Postnatal Thymus Seeding Progenitors and Regulatory Dynamics of Differentiating Immature Thymocytes. Immunity *52*, 1088-1104 e1086. 10.1016/j.immuni.2020.03.019.
18. Le, J., Park, J.E., Ha, V.L., Luong, A., Branciamore, S., Rodin, A.S., Gogoshin, G., Li, F., Loh, Y.E., Camacho, V., et al. (2020). Single-Cell RNA-Seq Mapping of Human Thymopoiesis Reveals Lineage Specification Trajectories and a Commitment Spectrum in T Cell Development. Immunity *52*, 1105-1118 e1109. 10.1016/j.immuni.2020.05.010.
19. Shao, M., Hepler, C., Vishvanath, L., MacPherson, K.A., Busbuso, N.C., and Gupta, R.K. (2017). Fetal development of subcutaneous white adipose tissue is dependent on Zfp423. Mol Metab *6*, 111-124. 10.1016/j.molmet.2016.11.009.
20. Gabriely, I., Ma, X.H., Yang, X.M., Atzmon, G., Rajala, M.W., Berg, A.H., Scherer, P., Rossetti, L., and Barzilai, N. (2002). Removal of visceral fat prevents insulin resistance and glucose intolerance of aging: an adipokine-mediated process? Diabetes *51*, 2951-2958. 10.2337/diabetes.51.10.2951.
21. Huh, J.Y., Park, J., Kim, J.I., Park, Y.J., Lee, Y.K., and Kim, J.B. (2017). Deletion of CD1d in Adipocytes Aggravates Adipose Tissue Inflammation and Insulin Resistance in Obesity. Diabetes *66*, 835-847. 10.2337/db16-1122.
22. Zoico, E., Rubele, S., De Caro, A., Nori, N., Mazzali, G., Fantin, F., Rossi, A., and Zamboni, M. (2019). Brown and Beige Adipose Tissue and Aging. Front Endocrinol (Lausanne) *10*, 368. 10.3389/fendo.2019.00368.
23. Porter, J.W., Barnas, J.L., Welly, R., Spencer, N., Pitt, J., Vieira-Potter, V.J., and Kanaley, J.A. (2020). Age, Sex, and Depot-Specific Differences in Adipose-Tissue Estrogen Receptors in Individuals with Obesity. Obesity (Silver Spring) *28*, 1698-1707. 10.1002/oby.22888.
24. Varghese, M., Song, J., and Singer, K. (2021). Age and Sex: Impact on adipose tissue metabolism and inflammation. Mech Ageing Dev *199*, 111563. 10.1016/j.mad.2021.111563.
25. Langhi, L.G., Andrade, L.R., Shimabukuro, M.K., van Ewijk, W., Taub, D.D., Borojevic, R., and de Mello Coelho, V. (2015). Lipid-Laden Multilocular Cells in the Aging Thymus Are Phenotypically Heterogeneous. PLoS One *10*, e0141516. 10.1371/journal.pone.0141516.
26. Dixen, K., Basse, A.L., Murholm, M., Isidor, M.S., Hansen, L.H., Petersen, M.C., Madsen, L., Petrovic, N., Nedergaard, J., Quistorff, B., and Hansen, J.B. (2013). ERRgamma enhances UCP1 expression and fatty acid oxidation in brown adipocytes. Obesity (Silver Spring) *21*, 516-524. 10.1002/oby.20067.
27. Muller, S., Perdikari, A., Dapito, D.H., Sun, W., Wollscheid, B., Balaz, M., and Wolfrum, C. (2020). ESRRG and PERM1 Govern Mitochondrial Conversion in Brite/Beige Adipocyte Formation. Front Endocrinol (Lausanne) *11*, 387. 10.3389/fendo.2020.00387.

688 28. Jash, S., Banerjee, S., Lee, M.J., Farmer, S.R., and Puri, V. (2019). CIDEA
689 Transcriptionally Regulates UCP1 for Britening and Thermogenesis in Human Fat Cells.
690 iScience *20*, 73-89. 10.1016/j.isci.2019.09.011.
691 29. Montoya, M., and Del Val, M. (1999). Intracellular rate-limiting steps in MHC class I
692 antigen processing. J Immunol *163*, 1914-1922.
693 30. Kousa, A.I., Jahn, L., Zhao, K., Flores, A.E., Acenas, D., 2nd, Lederer, E., Argyropoulos,
694 K.V., Lemarquis, A.L., Granadier, D., Cooper, K., et al. (2024). Age-related epithelial
695 defects limit thymic function and regeneration. Nat Immunol *25*, 1593-1606.
696 10.1038/s41590-024-01915-9.
697 31. Seale, P., Kajimura, S., Yang, W., Chin, S., Rohas, L.M., Uldry, M., Tavernier, G.,
698 Langin, D., and Spiegelman, B.M. (2007). Transcriptional control of brown fat
699 determination by PRDM16. Cell Metab *6*, 38-54. 10.1016/j.cmet.2007.06.001.
700 32. Hinds, T.D., Jr., Kipp, Z.A., Xu, M., Yiannikouris, F.B., Morris, A.J., Stec, D.F., Wahli, W.,
701 and Stec, D.E. (2021). Adipose-Specific PPARalpha Knockout Mice Have Increased
702 Lipogenesis by PASK-SREBP1 Signaling and a Polarity Shift to Inflammatory
703 Macrophages in White Adipose Tissue. Cells *11*. 10.3390/cells11010004.
704 33. Holman, C.D., Sakers, A.P., Calhoun, R.P., Cheng, L., Fein, E.C., Jacobs, C., Tsai, L.,
705 Rosen, E.D., and Seale, P. (2024). Aging impairs cold-induced beige adipogenesis and
706 adipocyte metabolic reprogramming. bioRxiv. 10.1101/2023.03.20.533514.
707 34. Kim, K.H., Lee, K., Moon, Y.S., and Sul, H.S. (2001). A cysteine-rich adipose tissue-
708 specific secretory factor inhibits adipocyte differentiation. J Biol Chem *276*, 11252-
709 11256. 10.1074/jbc.C100028200.
710 35. Nehls, M., Kyewski, B., Messerle, M., Waldschutz, R., Schuddekopf, K., Smith, A.J., and
711 Boehm, T. (1996). Two genetically separable steps in the differentiation of thymic
712 epithelium. Science *272*, 886-889. 10.1126/science.272.5263.886.
713 36. Youm, Y.H., Yang, H., Sun, Y., Smith, R.G., Manley, N.R., Vandanmagsar, B., and Dixit,
714 V.D. (2009). Deficient ghrelin receptor-mediated signaling compromises thymic stromal
715 cell microenvironment by accelerating thymic adiposity. J Biol Chem *284*, 7068-7077.
716 10.1074/jbc.M808302200.
717 37. Simpson, J.G., Gray, E.S., and Beck, J.S. (1975). Age involution in the normal human
718 adult thymus. Clin Exp Immunol *19*, 261-265.
719 38. Pido-Lopez, J., Imami, N., and Aspinall, R. (2001). Both age and gender affect thymic
720 output: more recent thymic migrants in females than males as they age. Clin Exp
721 Immunol *125*, 409-413. 10.1046/j.1365-2249.2001.01640.x.
722 39. Sandstedt, M., Chung, R.W.S., Skoglund, C., Lundberg, A.K., Ostgren, C.J., Ernerudh,
723 J., and Jonasson, L. (2023). Complete fatty degeneration of thymus associates with
724 male sex, obesity and loss of circulating naive CD8(+) T cells in a Swedish middle-aged
725 population. Immun Ageing *20*, 45. 10.1186/s12979-023-00371-7.
726 40. Baran-Gale, J., Morgan, M.D., Maio, S., Dhalla, F., Calvo-Asensio, I., Deadman, M.E.,
727 Handel, A.E., Maynard, A., Chen, S., Green, F., et al. (2020). Ageing compromises
728 mouse thymus function and remodels epithelial cell differentiation. Elife *9*.
729 10.7554/eLife.56221.
730 41. Kumar, R., Langer, J.C., and Snoeck, H.W. (2006). Transforming growth factor-beta2 is
731 involved in quantitative genetic variation in thymic involution. Blood *107*, 1974-1979.
732 10.1182/blood-2005-04-1495.
733 42. Frontini, A., Rousset, S., Cassard-Doulcier, A.M., Zingaretti, C., Ricquier, D., and Cinti,
734 S. (2007). Thymus uncoupling protein 1 is exclusive to typical brown adipocytes and is
735 not found in thymocytes. J Histochem Cytochem *55*, 183-189. 10.1369/jhc.6A7013.2006.

736 43. Angueira, A.R., Sakers, A.P., Holman, C.D., Cheng, L., Arbocco, M.N., Shamsi, F.,
737 Lynes, M.D., Shrestha, R., Okada, C., Batmanov, K., et al. (2021). Defining the lineage
738 of thermogenic perivascular adipose tissue. Nat Metab *3*, 469-484. 10.1038/s42255-021-
739 00380-0.
740 44. Cawthorn, W.P., Scheller, E.L., and MacDougald, O.A. (2012). Adipose tissue stem cells
741 meet preadipocyte commitment: going back to the future. J Lipid Res *53*, 227-246.
742 10.1194/jlr.R021089.
743 45. Braissant, O., Foufelle, F., Scotto, C., Dauca, M., and Wahli, W. (1996). Differential
744 expression of peroxisome proliferator-activated receptors (PPARs): tissue distribution of
745 PPAR-alpha, -beta, and -gamma in the adult rat. Endocrinology *137*, 354-366.
746 10.1210/endo.137.1.8536636.
747 46. Peeters, A., and Baes, M. (2010). Role of PPARalpha in Hepatic Carbohydrate
748 Metabolism. PPAR Res *2010*. 10.1155/2010/572405.
749 47. Kersten, S., Seydoux, J., Peters, J.M., Gonzalez, F.J., Desvergne, B., and Wahli, W.
750 (1999). Peroxisome proliferator-activated receptor alpha mediates the adaptive response
751 to fasting. J Clin Invest *103*, 1489-1498. 10.1172/JCI6223.
752 48. Kroon, T., Harms, M., Maurer, S., Bonnet, L., Alexandersson, I., Lindblom, A., Ahnmark,
753 A., Nilsson, D., Gennemark, P., O'Mahony, G., et al. (2020). PPARgamma and
754 PPARalpha synergize to induce robust browning of white fat in vivo. Mol Metab *36*,
755 100964. 10.1016/j.molmet.2020.02.007.
756 49. Kissig, M., Ishibashi, J., Harms, M.J., Lim, H.W., Stine, R.R., Won, K.J., and Seale, P.
757 (2017). PRDM16 represses the type I interferon response in adipocytes to promote
758 mitochondrial and thermogenic programing. EMBO J *36*, 1528-1542.
759 10.15252/embj.201695588.
760 50. Peverelli, E., Ermetici, F., Corbetta, S., Gozzini, E., Avagliano, L., Zappa, M.A.,
761 Bulfamante, G., Beck-Peccoz, P., Spada, A., and Mantovani, G. (2013). PKA regulatory
762 subunit R2B is required for murine and human adipocyte differentiation. Endocr Connect
763 *2*, 196-207. 10.1530/EC-13-0049.
764 51. Harms, M.J., Ishibashi, J., Wang, W., Lim, H.W., Goyama, S., Sato, T., Kurokawa, M.,
765 Won, K.J., and Seale, P. (2014). Prdm16 is required for the maintenance of brown
766 adipocyte identity and function in adult mice. Cell Metab *19*, 593-604.
767 10.1016/j.cmet.2014.03.007.
768 52. Ellis, J.M., Li, L.O., Wu, P.C., Koves, T.R., Ilkayeva, O., Stevens, R.D., Watkins, S.M.,
769 Muoio, D.M., and Coleman, R.A. (2010). Adipose acyl-CoA synthetase-1 directs fatty
770 acids toward beta-oxidation and is required for cold thermogenesis. Cell Metab *12*, 53-
771 64. 10.1016/j.cmet.2010.05.012.
772 53. Kang, G.J., Park, J.H., Kim, H.J., Kim, E.J., Kim, B., Byun, H.J., Yu, L., Nguyen, T.M.,
773 Nguyen, T.H., Kim, K.S., et al. (2022). PRR16/Largen Induces Epithelial-Mesenchymal
774 Transition through the Interaction with ABI2 Leading to the Activation of ABL1 Kinase.
775 Biomol Ther (Seoul) *30*, 340-347. 10.4062/biomolther.2022.066.
776 54. Monteiro, M.C., Sanyal, M., Cleary, M.L., Sengenes, C., Bouloumie, A., Dani, C., and
777 Billon, N. (2011). PBX1: a novel stage-specific regulator of adipocyte development. Stem
778 Cells *29*, 1837-1848. 10.1002/stem.737.
779 55. Xia, T., Shen, Z., Cai, J., Pan, M., and Sun, C. (2020). ColXV Aggravates Adipocyte
780 Apoptosis by Facilitating Abnormal Extracellular Matrix Remodeling in Mice. Int J Mol Sci
781 *21*. 10.3390/ijms21030959.
782 56. Zhu, X., Wei, L., Bai, Y., Wu, S., and Han, S. (2017). FoxC1 promotes epithelial-
783 mesenchymal transition through PBX1 dependent transactivation of ZEB2 in esophageal
784 cancer. Am J Cancer Res *7*, 1642-1653.

785 57. Lambert, A.W., and Weinberg, R.A. (2021). Linking EMT programmes to normal and
786 neoplastic epithelial stem cells. Nat Rev Cancer *21*, 325-338. 10.1038/s41568-021-
787 00332-6.
788 58. Roh, H.C., Tsai, L.T.Y., Shao, M., Tenen, D., Shen, Y., Kumari, M., Lyubetskaya, A.,
789 Jacobs, C., Dawes, B., Gupta, R.K., and Rosen, E.D. (2018). Warming Induces
790 Significant Reprogramming of Beige, but Not Brown, Adipocyte Cellular Identity. Cell
791 Metab *27*, 1121-1137 e1125. 10.1016/j.cmet.2018.03.005.
792 59. Lee, S., Benvie, A.M., Park, H.G., Spektor, R., Harlan, B., Brenna, J.T., Berry, D.C., and
793 Soloway, P.D. (2022). Remodeling of gene regulatory networks underlying thermogenic
794 stimuli-induced adipose beiging. Commun Biol *5*, 584. 10.1038/s42003-022-03531-5.
795 60. Rajakumari, S., Wu, J., Ishibashi, J., Lim, H.W., Giang, A.H., Won, K.J., Reed, R.R., and
796 Seale, P. (2013). EBF2 determines and maintains brown adipocyte identity. Cell Metab
797 *17*, 562-574. 10.1016/j.cmet.2013.01.015.
798 61. Brown, E.L., Hazen, B.C., Eury, E., Wattez, J.S., Gantner, M.L., Albert, V., Chau, S.,
799 Sanchez-Alavez, M., Conti, B., and Kralli, A. (2018). Estrogen-Related Receptors
800 Mediate the Adaptive Response of Brown Adipose Tissue to Adrenergic Stimulation.
801 iScience *2*, 221-237. 10.1016/j.isci.2018.03.005.
802 62. Kirschner, K.M., Foryst-Ludwig, A., Gohlke, S., Li, C., Flores, R.E., Kintscher, U.,
803 Schupp, M., Schulz, T.J., and Scholz, H. (2022). Wt1 haploinsufficiency induces
804 browning of epididymal fat and alleviates metabolic dysfunction in mice on high-fat diet.
805 Diabetologia *65*, 528-540. 10.1007/s00125-021-05621-1.
806 63. Martinez-Estrada, O.M., Lettice, L.A., Essafi, A., Guadix, J.A., Slight, J., Velecela, V.,
807 Hall, E., Reichmann, J., Devenney, P.S., Hohenstein, P., et al. (2010). Wt1 is required
808 for cardiovascular progenitor cell formation through transcriptional control of Snail and E-
809 cadherin. Nat Genet *42*, 89-93. 10.1038/ng.494.
810 64. Essafi, A., Webb, A., Berry, R.L., Slight, J., Burn, S.F., Spraggon, L., Velecela, V.,
811 Martinez-Estrada, O.M., Wiltshire, J.H., Roberts, S.G., et al. (2011). A wt1-controlled
812 chromatin switching mechanism underpins tissue-specific wnt4 activation and
813 repression. Dev Cell *21*, 559-574. 10.1016/j.devcel.2011.07.014.
814 65. Tontonoz, P., Hu, E., and Spiegelman, B.M. (1994). Stimulation of adipogenesis in
815 fibroblasts by PPAR gamma 2, a lipid-activated transcription factor. Cell *79*, 1147-1156.
816 10.1016/0092-8674(94)90006-x.
817 66. Michelson, D.A., Hase, K., Kaisho, T., Benoist, C., and Mathis, D. (2022). Thymic
818 epithelial cells co-opt lineage-defining transcription factors to eliminate autoreactive T
819 cells. Cell *185*, 2542-2558 e2518. 10.1016/j.cell.2022.05.018.
820 67. Mandel-Brehm, C., Vazquez, S.E., Liverman, C., Cheng, M., Quandt, Z., Kung, A.F.,
821 Parent, A., Miao, B., Disse, E., Cugnet-Anceau, C., et al. (2023). Autoantibodies to
822 Perilipin-1 Define a Subset of Acquired Generalized Lipodystrophy. Diabetes *72*, 59-70.
823 10.2337/db21-1172.
824 68. Agarwal, S., Bodansky, A., Xing, C., Anderson, M.S., and Garg, A. (2024). Partial
825 Lipodystrophy Affecting the Extremities in a Young Woman With Autoimmune
826 Polyglandular Syndrome 1. JCEM Case Rep *2*, luae166. 10.1210/jcemcr/luae166.
827 69. Yang, H., Youm, Y.H., Sun, Y., Rim, J.S., Galban, C.J., Vandanmagsar, B., and Dixit,
828 V.D. (2009). Axin expression in thymic stromal cells contributes to an age-related
829 increase in thymic adiposity and is associated with reduced thymopoiesis independently
830 of ghrelin signaling. J Leukoc Biol *85*, 928-938. 10.1189/jlb.1008621.
831 70. Yang, H., Youm, Y.H., Vandanmagsar, B., Rood, J., Kumar, K.G., Butler, A.A., and Dixit,
832 V.D. (2009). Obesity accelerates thymic aging. Blood *114*, 3803-3812. 10.1182/blood-
833 2009-03-213595.

71. Sheridan, J.M., Keown, A., Policheni, A., Roesley, S.N.A., Rivlin, N., Kadouri, N., Ritchie, M.E., Jain, R., Abramson, J., Heng, T.S.P., and Gray, D.H.D. (2017). Thymospheres Are Formed by Mesenchymal Cells with the Potential to Generate Adipocytes, but Not Epithelial Cells. Cell Rep *21*, 934-942. 10.1016/j.celrep.2017.09.090.
72. Venables, T., Griffith, A.V., DeAraujo, A., and Petrie, H.T. (2019). Dynamic changes in epithelial cell morphology control thymic organ size during atrophy and regeneration. Nat Commun *10*, 4402. 10.1038/s41467-019-11879-2.
73. Givony, T., Leshkowitz, D., Del Castillo, D., Nevo, S., Kadouri, N., Dassa, B., Gruper, Y., Khalaila, R., Ben-Nun, O., Gome, T., et al. (2023). Thymic mimetic cells function beyond self-tolerance. Nature *622*, 164-172. 10.1038/s41586-023-06512-8.
74. Zhu, X., Gui, J., Dohkan, J., Cheng, L., Barnes, P.F., and Su, D.M. (2007). Lymphohematopoietic progenitors do not have a synchronized defect with age-related thymic involution. Aging Cell *6*, 663-672. 10.1111/j.1474-9726.2007.00325.x.
75. Oh, J., Wang, W., Thomas, R., and Su, D.M. (2020). Thymic rejuvenation via FOXN1-reprogrammed embryonic fibroblasts (FREFs) to counteract age-related inflammation. JCI Insight *5*. 10.1172/jci.insight.140313.
76. Kim, M.J., Miller, C.M., Shadrach, J.L., Wagers, A.J., and Serwold, T. (2015). Young, proliferative thymic epithelial cells engraft and function in aging thymuses. J Immunol *194*, 4784-4795. 10.4049/jimmunol.1403158.
77. Bredenkamp, N., Nowell, C.S., and Blackburn, C.C. (2014). Regeneration of the aged thymus by a single transcription factor. Development *141*, 1627-1637. 10.1242/dev.103614.
78. Stuart, T., Butler, A., Hoffman, P., Hafemeister, C., Papalexi, E., Mauck, W.M., 3rd, Hao, Y., Stoeckius, M., Smibert, P., and Satija, R. (2019). Comprehensive Integration of Single-Cell Data. Cell *177*, 1888-1902 e1821. 10.1016/j.cell.2019.05.031.
79. Stuart, T., Srivastava, A., Madad, S., Lareau, C.A., and Satija, R. (2021). Single-cell chromatin state analysis with Signac. Nat Methods *18*, 1333-1341. 10.1038/s41592-021-01282-5.
80. Sergushichev, A.A. (2016). An algorithm for fast preranked gene set enrichment analysis using cumulative statistic calculation. bioRxiv *060012*. https://doi.org/10.1101/060012.

Figure 1

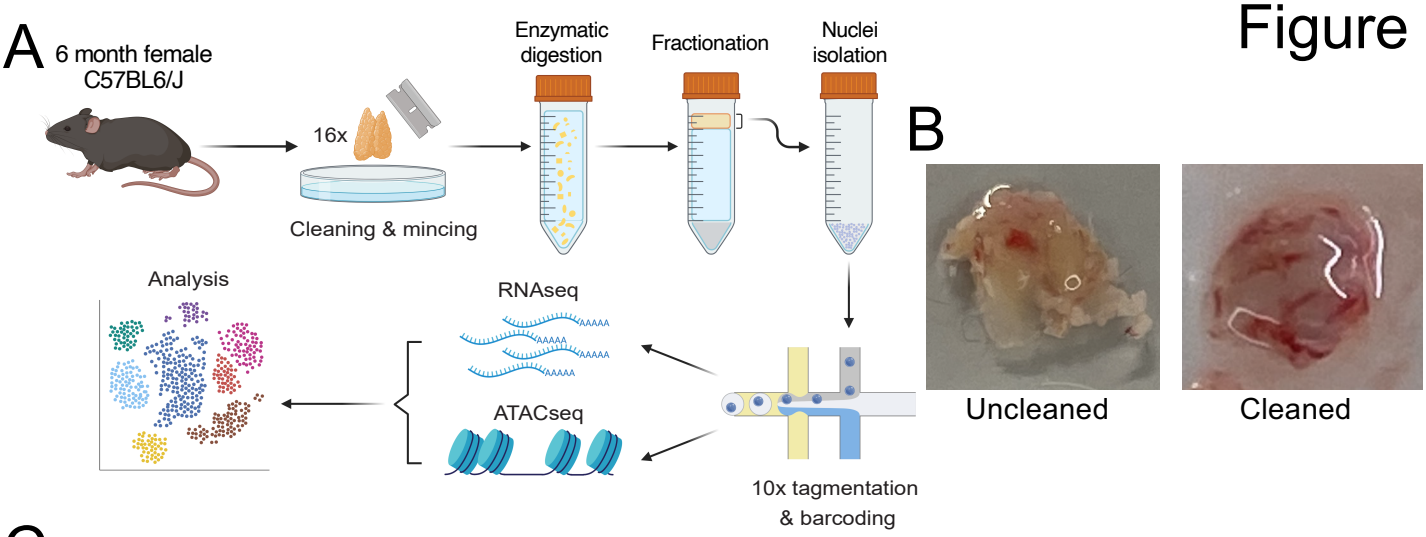
A
6 month female
C57BL6/J
16x
Cleaning & mincing
Enzymatic digestion
Fractionation
Nuclei isolation
Analysis
RNAseq
ATACseq
10x tagmentation & barcoding
B
Uncleaned
Cleaned

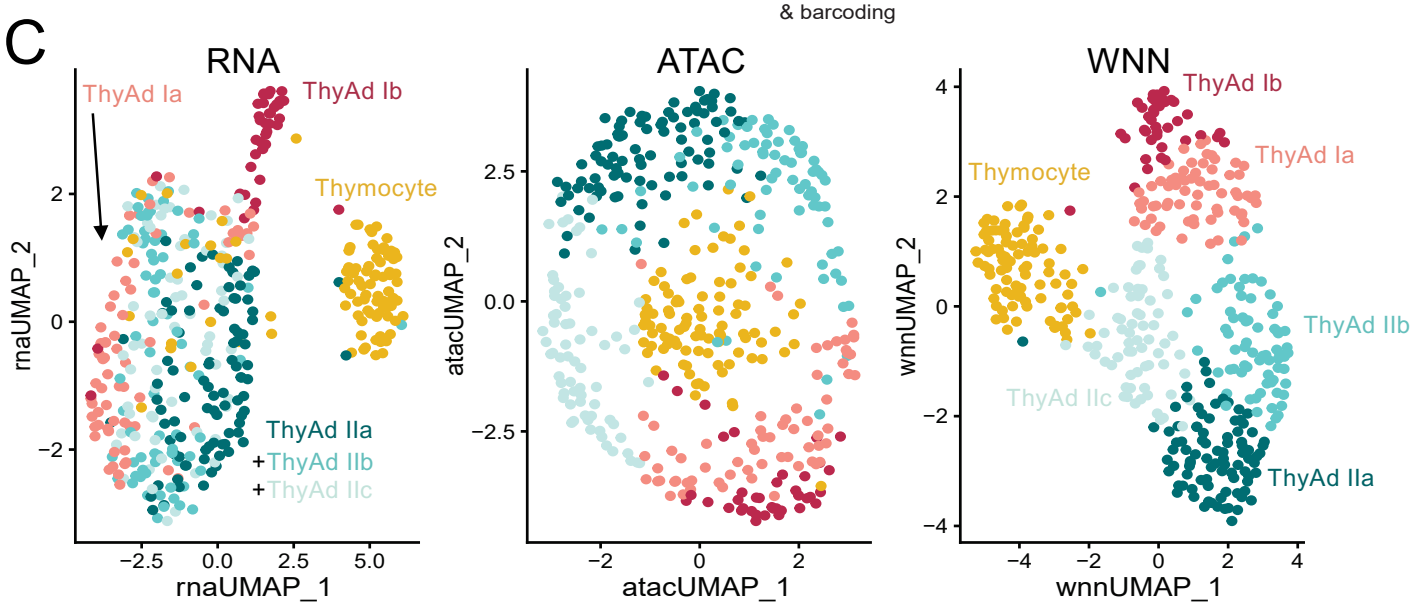
C
RNA
ATAC
WNN
ThyAd Ia
ThyAd Ib
Thymocyte
ThyAd IIa
+ThyAd IIb
+ThyAd IIc
ThyAd IIb
ThyAd IIc
rnaUMAP_1
rnaUMAP_2
atacUMAP_1
atacUMAP_2
wnnUMAP_1
wnnUMAP_2

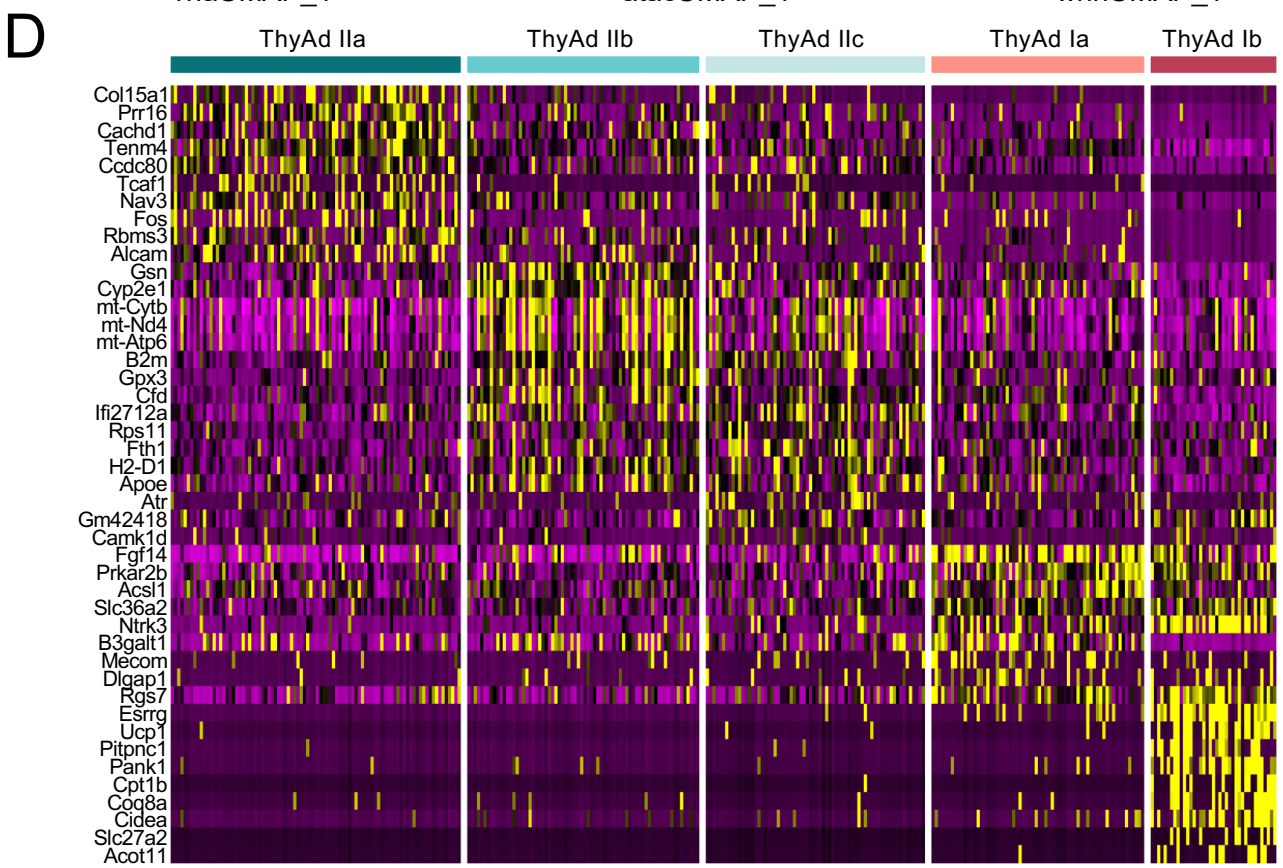
D
ThyAd IIa
ThyAd IIb
ThyAd IIc
ThyAd Ia
ThyAd Ib
Col15a1
Prr16
Cachd1
Tenm4
Ccdc80
Tcaf1
Nav3
Fos
Rbms3
Alcam
Gsn
Cyp2e1
mt-Cytb
mt-Nd4
mt-Atp6
B2m
Gpx3
Cfd
Ifi2712a
Rps11
Fth1
H2-D1
Apoe
Atr
Gm42418
Camk1d
Fgf14
Prkar2b
Acsl1
Slc36a2
Ntrk3
B3galt1
Mecom
Dlgap1
Rgs7
Esrrg
Ucp1
Pitpnc1
Pank1
Cpt1b
Coq8a
Cidea
Slc27a2
Acot11

Figure 2

A

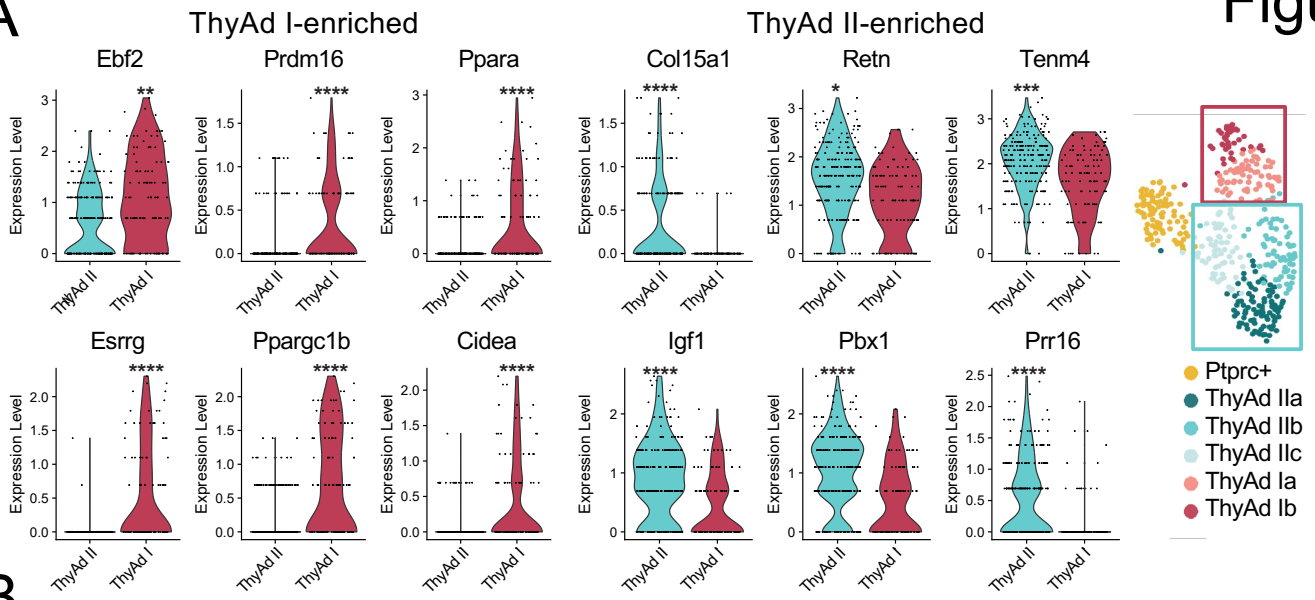

B

ThyAd I GO-Biological Process	NES	pval
Apoptotic mitochondrial changes	2.87	5.5E-04
Regulation of membrane potential	2.69	5.7E-04
Mitochondrial organization	2.39	7.8E-04
Regulation of anatomical structure morphogenesis	2.37	6.4E-04
Positive regulation of cold induced thermogenesis	2.30	4.9E-03
Sensory organ development	2.28	4.7E-03
Defense response to other organism	2.26	3.2E-03
Learning	2.26	9.5E-03
Regulation of lipid metabolic process	2.15	5.8E-03
Electron transport chain	2.12	9.6E-03
Regulation of cell projection organization	2.08	4.6E-03
ThyAd I GO-Hallmark	**NES**	**pval**
Estrogen response early	2.40	5.6E-03
Adipogenesis	2.24	4.3E-03

ThyAd II GO-Biological Process	NES	pval
Cell adhesion	2.68	1.9E-05
Extrinsic apoptotic signaling pathway	2.63	1.5E-03
Regulation of endothelial cell migration	2.61	5.0E-04
Negative regulation of developmental process	2.45	3.1E-04
Response to inorganic substance	2.30	2.2E-03
ATP synthesis coupled electron transport	2.30	5.4E-03
Regulation of locomotion	2.27	5.1E-04
Positive regulation of cellular catabolic process	2.16	9.9E-03
Regulation of cell population proliferation	2.02	3.4E-03
ThyAd II GO-Hallmark	**NES**	**pval**
Bile acid metabolism	2.26	6.6E-03
Epithelial mesenchymal transition	2.25	7.2E-03

Figure 3

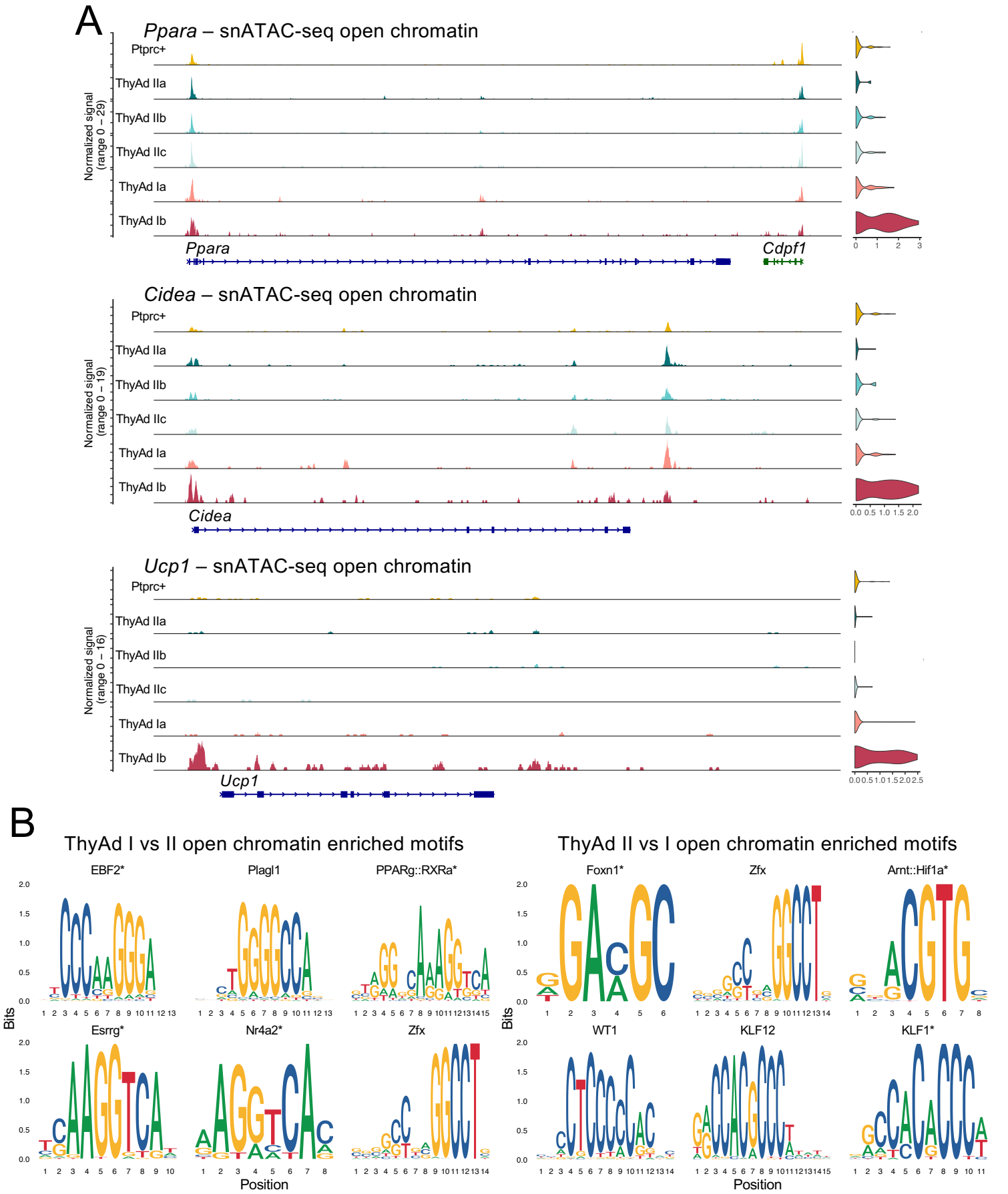
A
Ppara – snATAC-seq open chromatin
Ptprc+
ThyAd IIa
ThyAd IIb
ThyAd IIc
ThyAd Ia
ThyAd Ib
Normalized signal (range 0 – 29)
Ppara
Cdpf1
Cidea – snATAC-seq open chromatin
Normalized signal (range 0 – 19)
Cidea
Ucp1 – snATAC-seq open chromatin
Normalized signal (range 0 – 16)
Ucp1
B
ThyAd I vs II open chromatin enriched motifs
EBF2*
Plagl1
PPARg::RXRa*
Esrrg*
Nr4a2*
Zfx
ThyAd II vs I open chromatin enriched motifs
Foxn1*
Zfx
Arnt::Hif1a*
WT1
KLF12
KLF1*
Bits
Position

Figure 4

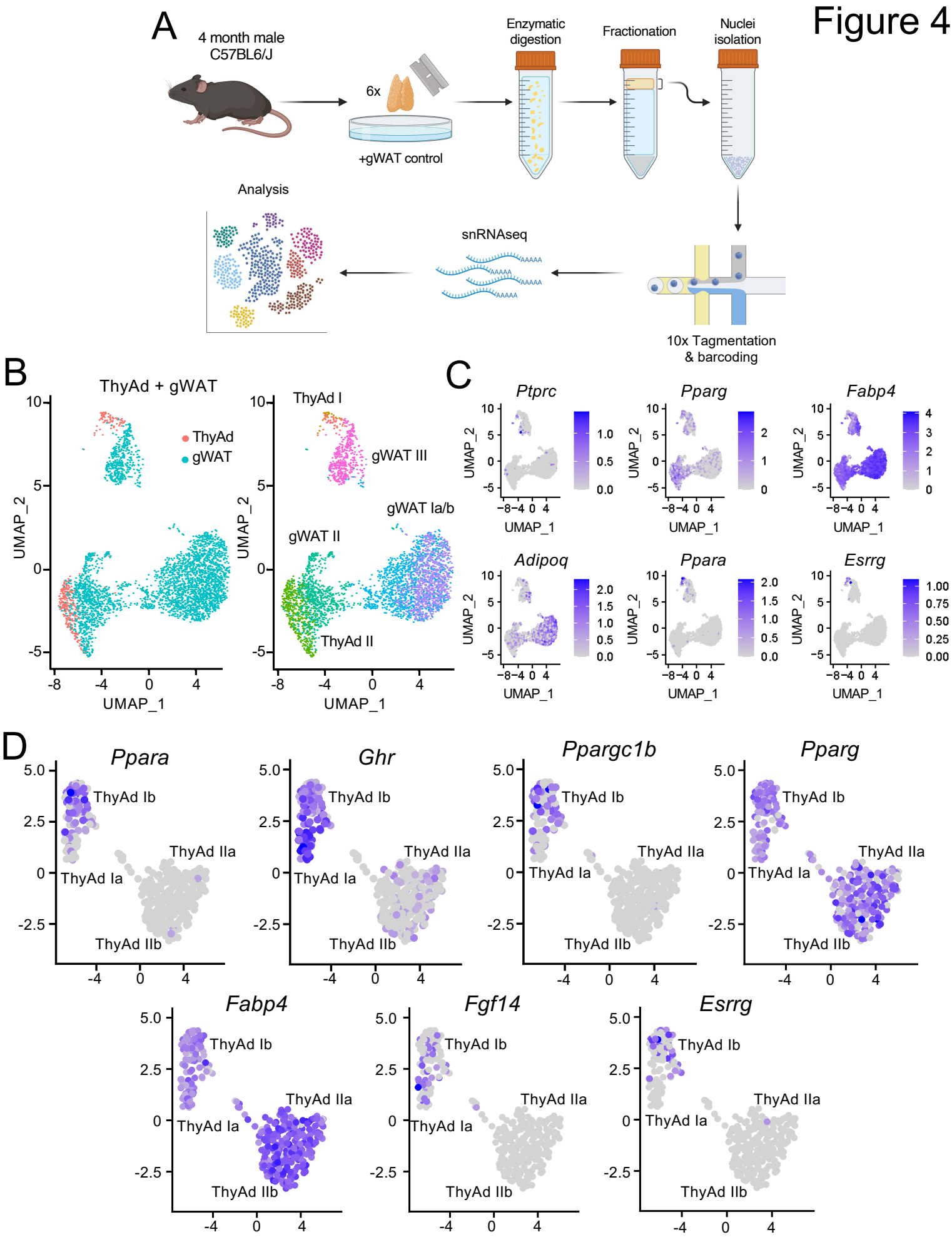
A
4 month male
C57BL6/J
6x
+gWAT control
Enzymatic
digestion
Fractionation
Nuclei
isolation
10x Tagmentation
& barcoding
snRNAseq
Analysis
B
ThyAd + gWAT
ThyAd
gWAT
ThyAd I
gWAT III
gWAT Ia/b
gWAT II
ThyAd II
UMAP_1
UMAP_2
C
Ptprc
Pparg
Fabp4
Adipoq
Ppara
Esrrg
D
Ppara
Ghr
Ppargc1b
Pparg
Fabp4
Fgf14
Esrrg
ThyAd Ib
ThyAd Ia
ThyAd IIa
ThyAd IIb

Figure 5

A

Minus 1° antibody

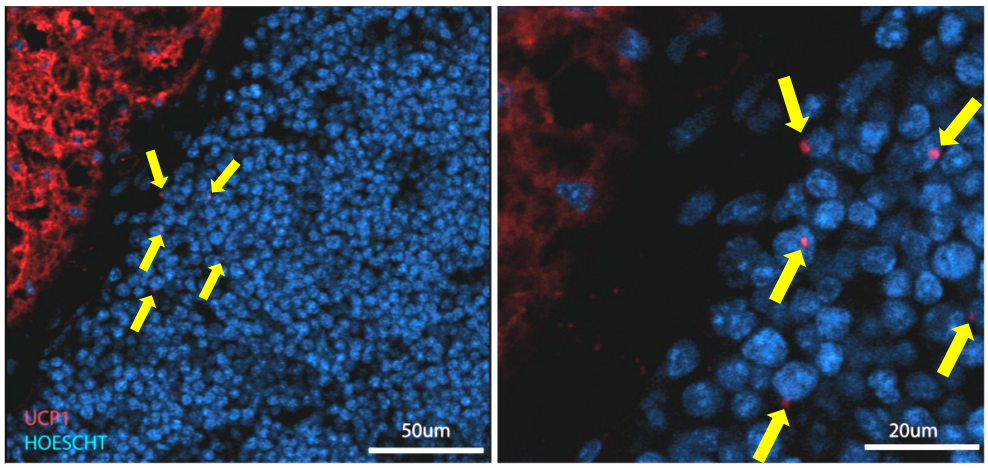

Adjacent section With 1° antibody

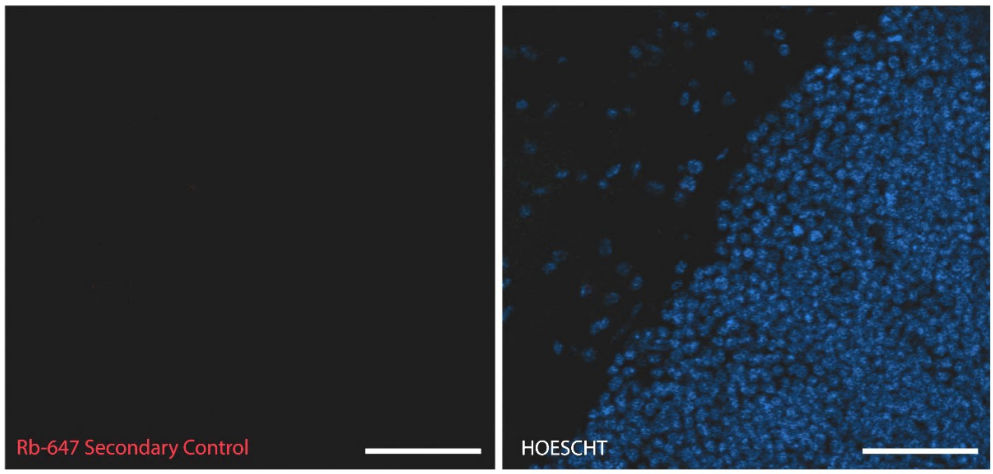

B

Minus 1° antibody

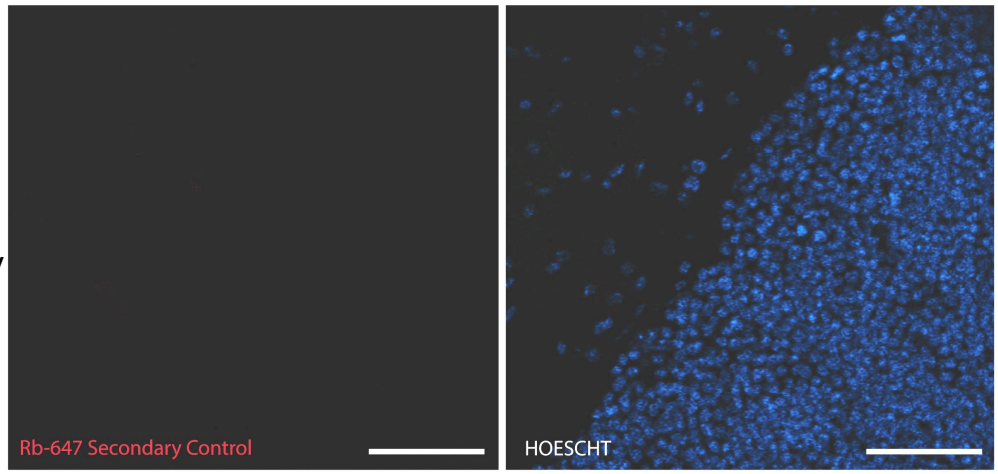
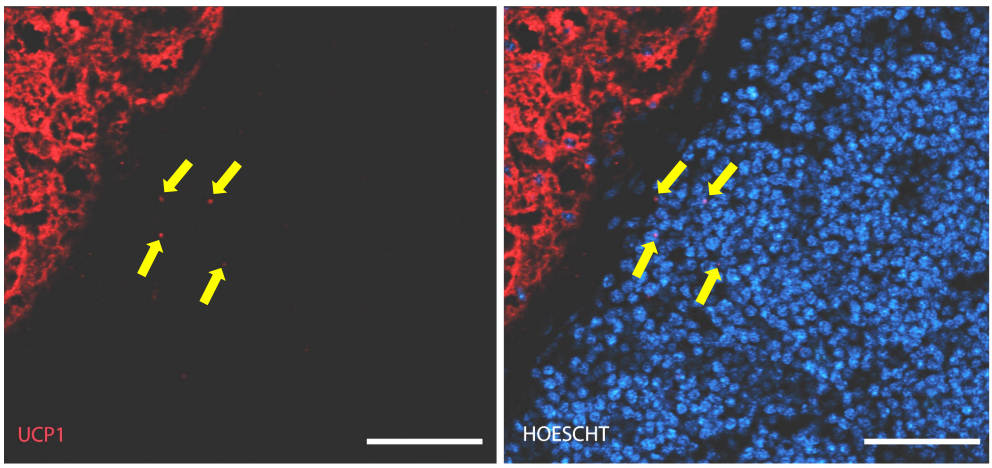
Adjacent section With 1° antibody